Magnetic Design for Three-Phase Dynamic Wireless Power Transfer with Constant Output Power

SUBMISSION DATE / POSTED DATE

28-04-2022 / 02-05-2022

CITATION

Brovont, Aaron; Aliprantis, Dionysios; Pekarek, Steven (2022): Magnetic Design for Three-Phase Dynamic Wireless Power Transfer with Constant Output Power. TechRxiv. Preprint.
https://doi.org/10.36227/techrxiv.19653372.v1

DOI

10.36227/techrxiv.19653372.v1

Magnetic Design for Three-Phase Dynamic Wireless Power Transfer with Constant Output Power

Aaron D. Brovont, *Member, IEEE,* Dionysios Aliprantis, *Senior Member, IEEE,*
and Steven D. Pekarek, *Fellow, IEEE*

***Abstract*—This paper details the design of a three-phase transmitter-receiver topology for use in a dynamic wireless power transfer (DWPT) system for heavy-duty electric vehicles. The proposed approach and topology eliminate the power oscillation and voltage/current sharing problems that plague planar three-phase DWPT systems. Multi-objective optimization is employed to maximize magnetic coupling and minimize undesired positive–negative sequence coupling, yielding a Pareto-optimal front that delineates the tradeoff between the two objectives for the proposed topology. Selected designs are simulated for a 200-kW/m DWPT system, verifying the elimination of power oscillation and phase imbalance with minimal impact on magnetic performance.**

I. Introduction

CLIMATE change concerns and major advances in power electronics are driving the rapid development of dynamic wireless power transfer (DWPT) systems. In particular, significant benefits lie with deploying DWPT technology for heavy-duty vehicle fleets. It is difficult to accommodate the power needs of heavy-duty electric vehicles with single-phase topologies; therefore, three-phase solutions are of interest.

The arrangement of the three-phase transmitter (tx) and receiver (rx) coils considered herein is shown in Fig. 1. In this planar topology, the magnetic poles travel transversely to the road. An advantage of this configuration is that it can be readily scaled lengthwise to meet a range of power ratings. However, a noted shortcoming is magnetic imbalance, leading to power oscillation and poor current/voltage sharing among phases. Prior efforts to balance the phases have focused on reducing interphase mutual couplings or adding external compensation [1], [2]. Demonstrated solutions tend to increase system cost/complexity or yield unsatisfactory performance.

Herein, it is shown that reducing or uniformly balancing mutual couplings in a three-phase DWPT system is not necessary to achieve constant power throughput and good current/voltage sharing. Specifically, a symmetrical components (SC)-based transformation of the inductance matrix for a generic pair of three-phase coils yields a T-equivalent circuit with explicit voltage source terms responsible for phase imbalance. Then, it is shown that these sequence-coupling terms may be eliminated through the design of the tx/rx coil layouts, even for a planar arrangement of coils and without highly permeable magnetic materials for flux shaping.

The design process involves a multi-objective optimization, which yields a set of tx/rx designs representing tradeoffs between maximizing magnetic coupling and minimizing sequence interaction. For illustration purposes, three designs are selected from the Pareto front, for which series-series compensation circuits and input/output conditions are determined to achieve 200 kW/m of average power output. The expected reduction in power oscillation and phase imbalance is verified through computer simulation of the resulting systems.

This material is based upon work supported by the National Science Foundation under Grant No. 1941524 and by the Joint Transportation Research Program administered by the Indiana Department of Transportation and Purdue University.

II. Transmitter-Receiver Equivalent Circuit Model

The flux linkage equations for a generic three-phase tx-rx pair (in a magnetically linear system) may be expressed as

$$\begin{bmatrix} \boldsymbol{\Lambda}_t^{ABC} \\ \boldsymbol{\Lambda}_r^{abc} \end{bmatrix} = \begin{bmatrix} \mathbf{L}_t & \mathbf{M}_{tr} \\ (\mathbf{M}_{tr})^\top & \mathbf{L}_r \end{bmatrix} \begin{bmatrix} \boldsymbol{I}_t^{ABC} \\ \boldsymbol{I}_r^{abc} \end{bmatrix} \tag{1}$$

in which the uppercase flux linkage and current variables indicate phasors. The inductance matrix is symmetric positive-definite; otherwise, matrix elements are independent.

A classical approach to analyzing imbalance in three-phase ac circuits is the SC transformation [3]. By introducing a SC transformation matrix $\mathbf{A}$, unbalanced phase quantities in a three-phase system are decomposed as a linear combination of balanced zero-sequence, positive-sequence, and negative-sequence phasor sets (denoted by a 012 superscript):

$$\boldsymbol{F}_x^{abc} \triangleq \mathbf{A}\boldsymbol{F}_x^{012}\,. \tag{2}$$

To apply SC to the flux linkage equations (1), we left-multiply the tx/rx equations by $\mathbf{A}^{-1}$, and utilize (2), leading to

$$\begin{bmatrix} \boldsymbol{\Lambda}_t^{012} \\ \boldsymbol{\Lambda}_r^{012} \end{bmatrix} = \begin{bmatrix} \mathbf{L}_t^{012} & \mathbf{M}_{tr}^{012} \\ (\mathbf{M}_{tr}^{012})^* & \mathbf{L}_r^{012} \end{bmatrix} \begin{bmatrix} \boldsymbol{I}_t^{012} \\ \boldsymbol{I}_r^{012} \end{bmatrix}. \tag{3}$$

Because the inductance matrix in (1) is real, the transformed diagonal submatrices are Hermitian, and the off-diagonal submatrices are conjugate-transposes of one another. Thus, the inductance matrix transformed into SC is also Hermitian.

We note the following regarding (3). First, for any real matrix $\mathbf{P}$ transformed as $\mathbf{A}^{-1}\mathbf{P}\mathbf{A}$, it can be shown that the positive- and negative-sequence diagonal elements are complex conjugates. Hence, $L_t^{22} = L_t^{11*}$, $L_r^{22} = L_r^{11*}$, and $M_{tr}^{22} = M_{tr}^{11*}$. Since

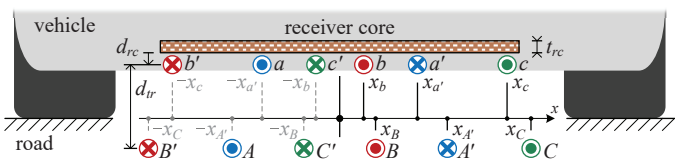

Fig. 1. Archetypal cross-section of proposed three-phase tx/rx topology.

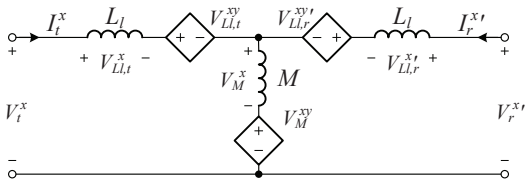

Fig. 2. SC sequence T-equivalent model of a generic 3-phase tx/rx system.

the self-inductance submatrices, $\mathbf{L}_t^{012}$ and $\mathbf{L}_r^{012}$, are Hermitian, we can define real-valued tx/rx sequence self-inductances

$$L_T \triangleq L_t^{11} = L_t^{22} \in \mathbb{R}, \quad L_R \triangleq L_r^{11} = L_r^{22} \in \mathbb{R}. \tag{4}$$

Second, it can be shown that the positive–negative-sequence off-diagonal elements are complex conjugates: i.e., $L_t^{21} = L_t^{12*}$, $L_r^{21} = L_r^{12*}$, and $M_{tr}^{21} = M_{tr}^{12*}$. Third, it is convenient to refer the rx-side quantities to the tx side as is typical for transformers, using the "turns ratio" factor: $n \triangleq \sqrt{L_R/L_T}$ [4]. Fourth, the imaginary parts of M_{tr}^{11} and M_{tr}^{22} are negligible for the topology considered herein. We can therefore define a real-valued sequence mutual inductance

$$M \triangleq \mathrm{Re}\{M_{tr}^{11\prime}\} = \mathrm{Re}\{M_{tr}^{22\prime}\}\,. \tag{5}$$

Finally, it is assumed that the zero sequence can be neglected for the purpose of analyzing power transfer. Under these conditions and simplifications, the positive-sequence equations of (3) can be expressed as

$$\begin{bmatrix} \Lambda_t^1 \\ \Lambda_r^{1\prime} \end{bmatrix} = \begin{bmatrix} L_T & M \\ M & L_T \end{bmatrix} \begin{bmatrix} I_t^1 \\ I_r^{1\prime} \end{bmatrix} + \begin{bmatrix} L_t^{12} & M_{tr}^{12\prime} \\ M_{tr}^{12\prime} & L_r^{12\prime} \end{bmatrix} \begin{bmatrix} I_t^2 \\ I_r^{2\prime} \end{bmatrix}. \tag{6}$$

The negative-sequence equations are identical in form, except that positive- and negative-sequence variables exchange places, and all matrix elements are conjugated.

To avoid interaction between positive- and negative-sequences, it is necessary to eliminate the inductances in the second matrix of (6). To this end, we derive the sequence T-equivalent circuits and express the undesired couplings in a normalized form. Let leakage inductance be defined as

$$L_l \triangleq L_T - M. \tag{7}$$

Splitting the tx/rx self-flux linkages in (6) into leakage and magnetizing components using the definitions in (5) and (7) yields the equations corresponding to a typical T-equivalent circuit with additional undesired terms representing sequence interaction. These sequence-coupling terms may be expressed in terms of voltages with normalized coefficients by defining leakage and magnetizing flux linkages as

$$\Lambda_{Ll,t}^x \triangleq L_l I_t^x, \quad \Lambda_M^x \triangleq M(I_t^x + I_r^{x\prime}), \quad \Lambda_{Ll,r}^{x\prime} \triangleq L_l I_r^{x\prime}, \tag{8}$$

where $x \in \{1, 2\}$. Finally, replacing the negative-sequence currents of (6) with corresponding expressions from (8) yields:

$$\Lambda_t^1 = L_l I_t^1 + M(I_t^1 + I_r^{1\prime}) + \frac{L_t^{12} - M_{tr}^{12\prime}}{L_l}\Lambda_{Ll,t}^2 + \frac{M_{tr}^{12\prime}}{M}\Lambda_M^2\,, \tag{9}$$

$$\Lambda_r^{1\prime} = L_l I_r^{1\prime} + M(I_t^1 + I_r^{1\prime}) + \frac{L_r^{12\prime} - M_{tr}^{12\prime}}{L_l}\Lambda_{Ll,r}^{2\prime} + \frac{M_{tr}^{12\prime}}{M}\Lambda_M^2. \tag{10}$$

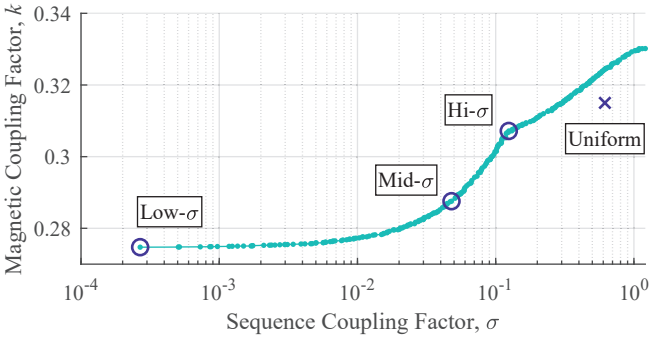

Fig. 3. Pareto-optimal front delineating the tradeoff between tx–rx coupling and sequence interaction.

Equations (9) and (10) imply a T-equivalent circuit of the form shown in Fig. 2, where $V = j\omega\Lambda$. (Resistances are not included for clarity.)

III. Optimization of Coil Geometry

A design optimization problem is posed to show that it is practicable to reduce sequence interaction for planar windings without significant magnetic performance degradation. Specifically, to eliminate the sequence coupling in the magnetizing branch of Fig. 2, the coefficient $M_{tr}^{12\prime}/M$ must vanish. Assuming this is feasible, (9) and (10) indicate that the remaining factors to minimize are L_t^{12}/L_l and $L_r^{12\prime}/L_l$. To aid optimization convergence, it is helpful to define a unitless "sequence-coupling factor" to be minimized, which represents the aggregate effect of these undesirable terms:

$$\sigma \triangleq \frac{\left|M_{tr}^{12\prime}\right|}{M} + \frac{\left|L_t^{12}\right|}{L_l} + \frac{\left|L_r^{12\prime}\right|}{L_l}. \tag{11}$$

A common metric for DWPT magnetic performance, which we wish to maximize, is the coupling factor:

$$k \triangleq M/L_T\,, \tag{12}$$

which is based on the definitions of (4) and (5).

Let $\mathbf{x}$ be a vector of geometric parameters defining a candidate design, as indicated in Fig. 1. Here, the two-objective design problem is: $\arg\max_{\mathbf{x}} \{\sigma^{-1}, k\}$. This optimization problem was solved using an evolutionary computing toolbox [5]. The tx-rx inductance matrix in (1) was computed for each candidate design (assuming perfect alignment) using the boundary element method [6].

As an illustrative case study, an optimization was performed to design tx-rx pairs on a per-turn, per-length basis. The coil distance d_{tr} was set to 21 cm, and the rx/tx widths were constrained so as not to exceed 0.9 m and 1.2 m, respectively. The receiver core was specified to be MN60 ferrite with thickness $t_{rc} = 1$ cm. The optimization produced the Pareto-optimal front shown in Fig. 3. The performance metrics of a "uniform" conductor arrangement (spaced equally across the full widths of the tx/rx) are also plotted therein.

The placement of coils yielding the optimal tradeoff between k and σ is plotted in Fig. 4. To maximize tx–rx coupling, the winding layouts tend to take up the full permitted widths. In

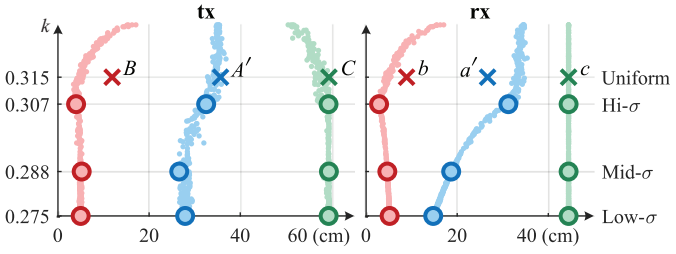

Fig. 4. Right-half plane conductor placement for optimal and uniform designs.

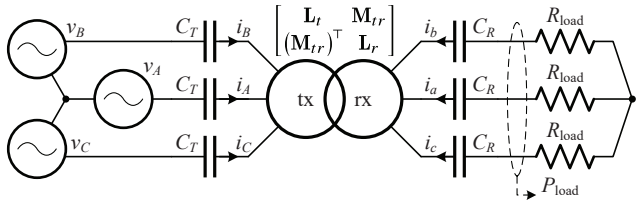

Fig. 5. System employed for validation simulations.

contrast, to reduce sequence interaction, the interior coil-sides crowd to the center. It can be shown that σ vanishes if

$$L_A + 2L_{BC} = L_B + 2L_{CA} = L_C + 2L_{AB}\,, \tag{13a}$$

$$L_a + 2L_{bc} = L_b + 2L_{ca} = L_c + 2L_{ab}\,, \tag{13b}$$

$$\begin{aligned} M_{Aa} + M_{Bc} + M_{Cb} &= M_{Bb} + M_{Ca} + M_{Ac} \\ &= M_{Cc} + M_{Ab} + M_{Ba}\,. \end{aligned} \tag{13c}$$

The inductance matrix for the "low-σ" design, reported below for reference, meets these constraints within the tolerance corresponding to the sequence-coupling factor:

$$\mathbf{L}_{tr} = \left[\begin{array}{ccc|ccc} 2.143 & -0.311 & -0.311 & 0.438 & -0.330 & -0.330 \\ -0.311 & 2.224 & -0.270 & -0.195 & 0.613 & -0.175 \\ -0.311 & -0.270 & 2.224 & -0.195 & -0.175 & 0.613 \\ \hline & & & 2.812 & -0.465 & -0.465 \\ & (\mathbf{M}_{tr})^\top & & -0.465 & 2.856 & -0.443 \\ & & & -0.465 & -0.443 & 2.856 \end{array}\right] \mu\text{H/m}. \tag{14}$$

IV. Verification of Optimal Designs

Simulations were performed to verify that the optimized designs reduce undesirable effects due to sequence interaction. The inductances calculated for the selected designs highlighted in Fig. 3 were used to populate the elementary system detailed in Fig. 5. A series-series compensation scheme was used to condition the input and output for each tx-rx pair [7], although it is noted that its sequence-interaction property is independent of the compensation circuit. The capacitors were sized according to $C_x = [(2\pi f_0)^2 L_x]^{-1}$ where $x \in \{T, R\}$ and $f_0 = 85$ kHz. Additionally, the load for each simulation was set to achieve equal input and output voltages (specifically, $R_{\text{load}} = 2\pi f_0 nM$). The input voltage sources were an ideal, three-phase, positive-sequence set with amplitude specified to achieve 200 kW/m average output power. The rms phase-to-neutral voltage amplitudes V_s used in the simulation studies are listed in Table I.

The simulated output power for the selected designs is plotted in Fig. 6, and key performance data are listed in Table I. The results indicate that the low-σ tx-rx design does

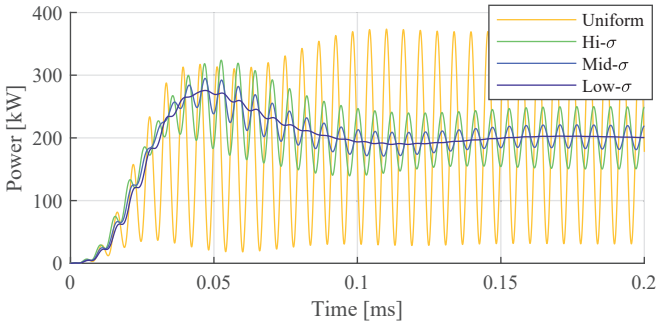

Fig. 6. Simulated power delivered to load for selected designs.

TABLE I
Design Verification Performance Parameters and Metrics

Design	k (pu)	σ (%)	V_s (Vrms/turn)	$\lvert\mathbf{I}_{ABC}\rvert$ (Arms·turns)	ΔP_{load} (%)
Uniform	0.315	61.6	152	{221, 587, 611}	84.4
Hi-σ	0.307	12.4	174	{287, 433, 431}	24.2
Mid-σ	0.288	4.79	170	{354, 410, 407}	9.21
Low-σ	0.275	0.0268	166	{398, 398, 398}	0.0425

indeed transfer power with minimal output ripple, which is a vast improvement over the higher-σ and uniform designs. Also, it can be seen that σ correlates well with the output power ripple ΔP_{load}. Additionally, the elimination of positive–negative sequence interaction balances the currents between the three phases, and reduces the maximum phase current by 35% relative to the uniform case.

V. Conclusion

This paper has presented an approach to design three-phase planar tx/rx coils for dynamic wireless power transfer that mitigates the deleterious impacts of phase imbalance. The resulting designs are strikingly simple while maintaining sufficient magnetic performance to meet the power targets for heavy-duty electric vehicles.

References

[1] M. L. G. Kissin, J. T. Boys, and G. A. Covic, "Interphase mutual inductance in polyphase inductive power transfer systems," *IEEE Trans. Ind. Electron.*, vol. 56, no. 7, pp. 2393–2400, Jul. 2009.

[2] A. Safaee, K. Woronowicz, and A. Maknouninejad, "Reactive power compensation scheme for an imbalanced three-phase series-compensated wireless power transfer system with a star-connected load," in *Proc. IEEE Int. Transport. Electrific. Conf., Expo*, Jun. 2018, pp. 44–48.

[3] E. Clarke, *Circuit analysis of AC power systems; symmetrical and related components*. Wiley, 1943, vol. 1.

[4] S. Li, W. Li, J. Deng, T. D. Nguyen, and C. C. Mi, "A double-sided LCC compensation network and its tuning method for wireless power transfer," *IEEE Trans. Veh. Technol.*, vol. 64, no. 6, pp. 2261–2273, Jun. 2015.

[5] S. Sudhoff, "Genetic Optimization System Engineering Tool (GOSET) for Use with MATLAB." [Online]. Available: https://engineering.purdue.edu/ECE/Research/Areas/PES

[6] A. D. Brovont and S. D. Pekarek, "Integral evaluation for a closed-form 2-D potential formulation of the Galerkin BEM," *Eng. Anal. Boundary Elements*, vol. 132, pp. 77–93, Nov. 2021.

[7] W. Li, H. Zhao, J. Deng, S. Li, and C. C. Mi, "Comparison study on SS and double-sided LCC compensation topologies for EV/PHEV wireless chargers," *IEEE Trans. Veh. Technol.*, vol. 65, no. 6, pp. 4429–4439, Jun. 2016.